Nanoscale

ROYAL SOCIETY OF CHEMISTRY

PAPER

View Article Online
View Journal | View Issue

Check for updates

**Cite this:** *Nanoscale*, 2024, **16**, 657

# Novel hollow $MoS_2$@C@$Cu_2S$ heterostructures for high zinc storage performance†

Yujin Li,[a,c] Jing Xu,*[a] Xinqi Luo,[a] Futing Wang,[c] Zhong Dong,[a] Ke-Jing Huang, *[b] Chengjie Hu,[a] Mengyi Hou[a] and Ren Cai *[c]

Received 17th October 2023,
Accepted 17th November 2023

DOI: 10.1039/d3nr05231a

rsc.li/nanoscale

Heterostructured materials have great potential as cathodes for zinc-ion batteries (ZIBs) because of their fast $Zn^{2+}$ transport channels. Herein, hollow $MoS_2$@C@$Cu_2S$ heterostructures are innovatively constructed using a template-engaged method. The carbon layer improves the electrical conductivity, provides a high *in situ* growth area, and effectively restricts volume expansion during the recycling process. $MoS_2$ nanosheets are grown on the surfaces of hollow C@$Cu_2S$ nanocubes using the *in situ* template method, further expanding the specific surface area and exposing more active sites to enhance the electrical conductivity. As expected, an admirable reversible capacity of 197.2 mA h $g^{-1}$ can be maintained after 1000 cycles with a coulombic efficiency of 91.1%. Therefore, we firmly believe that this work points the way forward for high-performance materials design and energy storage systems.

## Introduction

With the development of advanced energy storage technologies, lithium-ion batteries (LIBs) have exhibited some inevitable defects, such as high cost and potential safety hazards.[1–3] Currently, aqueous system zinc ion batteries (ZIBs) are expected to be alternatives to LIBs due to their low cost, abundant resources, and high security.[4,5] Although there have been many advances in the research on ZIBs, the design of high-performance ZIBs still faces great challenges, such as slow diffusion of zinc ions and low reversibility, which seriously hinder their development and commercialization.[6,7]

As a new type of 2D structure, many transition metal dichalcogenides (TMDs) are attracting attention as novel energy storage materials, because of their efficient energy conversion.[8–11] For example, $VS_4$@rGO nanosheets were explored using a hydrothermal process for super-performance ZIBs;[12] as a novel electrode, $WS_2$ nanosheets exhibited high specific capacity and were applied in sodium-ion batteries;[13] $SnS_2/Ti_3C_2T_x$ nanosheets were fabricated using an *in situ* hybridization method for high-performance potassium-ion batteries.[14] More interestingly, CuS nanocubes exhibited high energy density when used as cathode materials,[15] and $MoS_2$ nanosheets are conducive to ion intercalation/deintercalation in lithium/sodium-ion batteries.[16,17] However, there are some challenges in the application of $MoS_2$ nanosheets in ZIBs, such as poor conductivity, higher hydrophilicity, agglomeration, and volume expansion.[18–20] Therefore, it is important to explore novel $MoS_2$ structures with high conductivity and cycling stability for energy storage.

**Ren Cai**

*Dr. Ren Cai, a Professor at Hunan University, earned his Ph.D. in Analytical Chemistry from the University of Florida (USA) in 2017. Dr. Cai's research interests focus on novel analytical technologies, nanomedicine, and novel biosensors. At present, Dr. Cai has published over 70 peer-reviewed articles, including over 50 articles as the first author or corresponding author at J. Am. Chem. Soc., Anal. Chem., et al. Dr. Cai serves as the young editorial board of Collagen and Leather and Exploration, respectively.*

---

[a] College of Chemistry and Chemical Engineering, Xinyang Normal University, Xinyang 464000, China

[b] Education Department of Guangxi Zhuang Autonomous Region, Key Laboratory of Applied Analytical Chemistry, Guangxi Collaborative Innovation Center for Chemistry and Engineering of Forest Products, Guangxi Key Laboratory of Chemistry and Engineering of Forest Products, Key Laboratory of Chemistry and Engineering of Forest Products, State Ethnic Affairs Commission, School of Chemistry and Chemical Engineering, Guangxi Minzu University, Nanning 530006, China

[c] Molecular Science and Biomedicine Laboratory, State Key Laboratory for Chemo/Bio-Sensing and Chemometrics, College of Material Science and Engineering, College of Chemistry and Chemical Engineering, College of Biology, Hunan University, Changsha, 410082, China

† Electronic supplementary information (ESI) available. See DOI: **https://doi.org/10.1039/d3nr05231a**

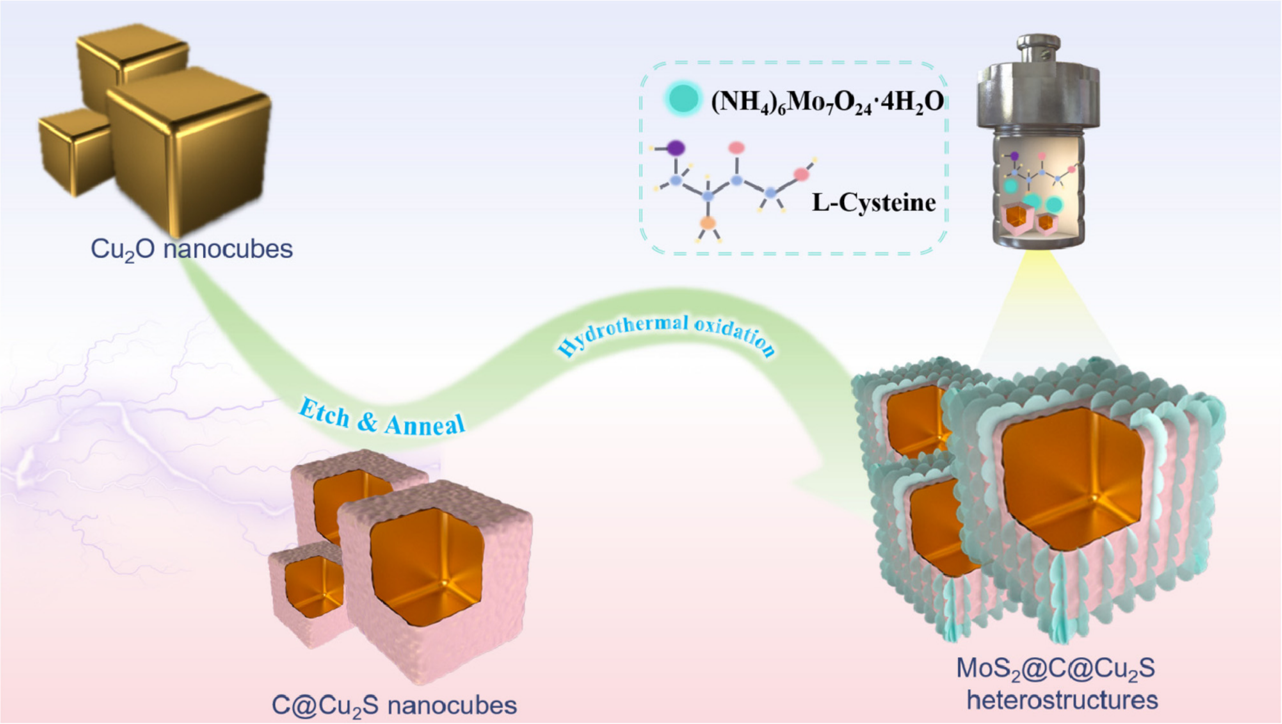

**Scheme 1** Synthetic process of the hollow $MoS_2$@C@$Cu_2S$ heterostructures.

Herein, we fabricated novel $MoS_2$@C@$Cu_2S$ heterostructures using a template-engaged process for high-capacity $Zn^{2+}$ storage (Scheme 1). These heterostructures are composed of $MoS_2$ nanosheets and hollow C@$Cu_2S$ nanocubes, and exhibit high specific surface area, exposing many active sites and enhancing the electrical conductivity in ZIBs. The hollow cavity facilitates rapid $Zn^{2+}$ transport to reduce the energy barrier of $Zn^{2+}$ absorption and transport, and reinforces the volume elasticity to accommodate volume change during $Zn^{2+}$ de-/intercalation. At current densities of 0.1 A $g^{-1}$ and 1.0 A $g^{-1}$, the as-designed ZIBs exhibit stable specific capacities of 679.1 mA h $g^{-1}$ and 192.9 mA h $g^{-1}$, respectively.

## Results and discussion

The hollow $MoS_2$@C@$Cu_2S$ heterostructures (size of ~600 nm) were prepared using an etching process followed by hydrothermal reduction (Scheme 1 and Fig. 1a and b). First, hollow CuS nanocubes with uniform sizes (size of ~500 nm, Fig. S1b†) were prepared by the reaction of $Cu_2O$ nanocubes (size of ~550 nm, Fig. S1a†), $Na_2S$, and HCl. After carbonization, PDA@CuS nanocubes converted into hollow C@$Cu_2S$ nanocubes (size of ~550 nm, Fig. S1c†). Finally, hollow heterostructures were prepared after folding $MoS_2$ nanosheets were grown on the surface of hollow C@$Cu_2S$ nanocubes (Fig. 1c).

The X-ray powder diffraction (XRD) pattern shows that all peaks of the crystal phases are indexed to $MoS_2$ (JCPDS: 37-1492) and $Cu_2S$ (JCPDS: 72-2276) (Fig. S2†). As exemplified in elemental distribution scanning (Fig. 1e), the distribution of C can be seen in the intermediate layer (Fig. S3†). These hollow CuS nanocubes with folding $MoS_2$ nanosheets and the C layer are $MoS_2$@C@$Cu_2S$ heterostructures. As further evidence, the lattice diffraction fringe at 0.606 nm corresponds to the (0 0 2) crystal plane of $MoS_2$, and the fringe at 0.260 nm corresponds to the (1 0 3) crystal plane of $Cu_2S$ in the high-resolution TEM image (Fig. 1d). X-ray photoelectron spectroscopy (XPS) further confirmed that the hollow heterostructure is composed of S, Mo, C, and Cu (Fig. S3†). The $E^1{}_{2g}$ and $A_{1g}$ peaks from $MoS_2$, the Cu–S vibration, and the D-band (defect vibration) and the G-band (graphitic carbon vibration) from C are observed in Raman spectroscopy (Fig. S4†), demonstrating the presence of $MoS_2$, CuS and the carbon layer in the heterostructures. In addition, the heterostructures show typical *meso*-shell structures with a large specific surface area of 34.10 $m^2$ $g^{-1}$ (Fig. S5†).

The electrochemical properties of the $MoS_2$@C@$Cu_2S$ heterostructures were investigated as shown in Fig. 2. As shown in Fig. 2a, the irreversible cathodic peaks at 0.32 V result from multiple electrochemical reactions, which involve the insertion of $Zn^{2+}$ to form $Zn_xCu_2S/Zn_xMoS_2$ and to generate ZnS and Mo. In the subsequent positive scan, the peak at 0.71 V corresponds to the dezincing of ZnS to re-generate $Cu_2S$ and $MoS_2$. Due to the formation of a solid electrolyte layer (SEI) film during the initial activation process, the loss of irre-

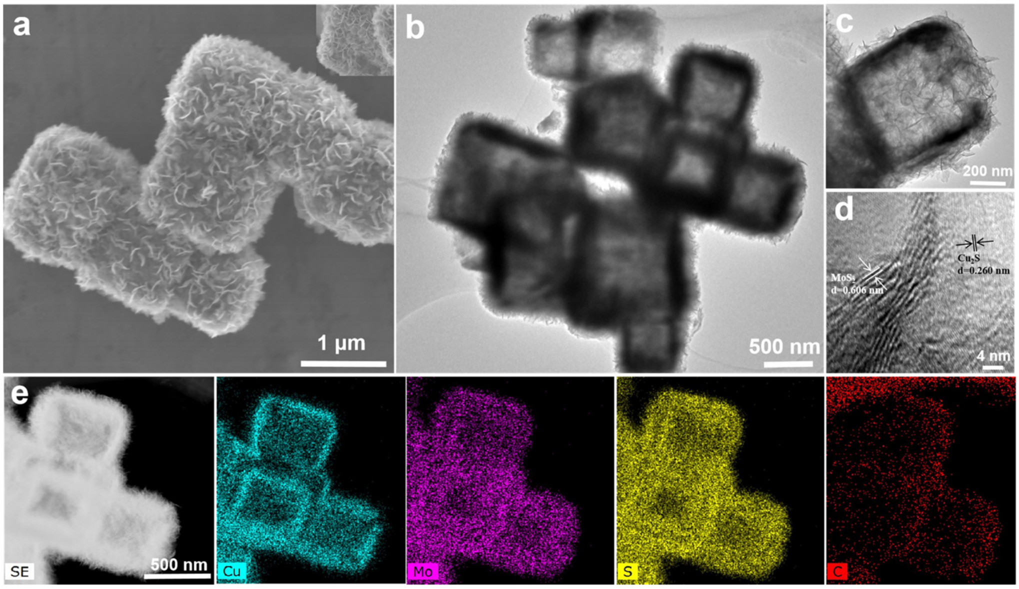

**Fig. 1** Characterization of $MoS_2$@C@$Cu_2S$ heterostructures: (a) SEM image; (b–d) TEM images; (e) elemental mapping images.

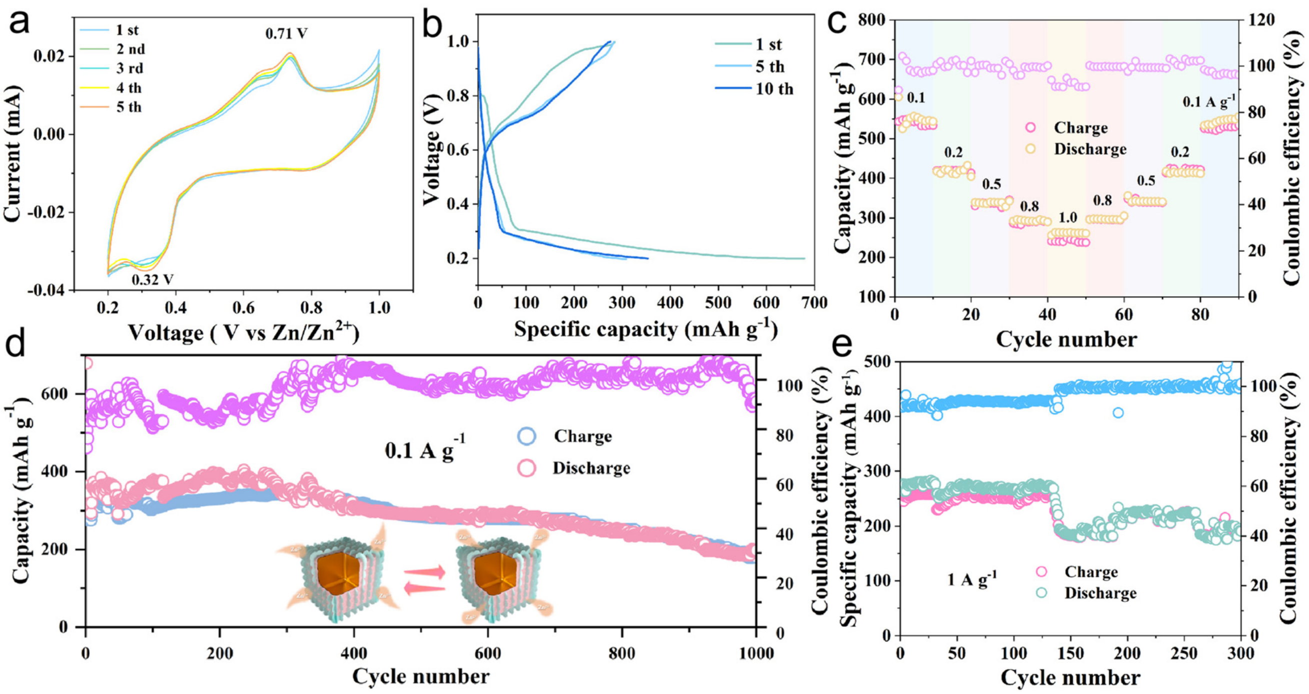

**Fig. 2** The electrochemical performance tests of $MoS_2$@C@$Cu_2S$ heterostructures: (a) CV profiles at 0.1 mV $s^{-1}$; (b) charge–discharge curves of the first, fifth and tenth cycles; (c) rate performance; (d) long-term cycling performance; (e) high current density performance.

versible capacity results in a larger area in the initial cycle than that in the following cycles. From the second cycle to the fifth cycle, the curves show good overlap, indicating good cycling stability.

In Fig. 2b, the galvanostatic charge–discharge (GCD) test exhibits the charge–discharge curves of the heterostructures at a current density of 0.1 A $g^{-1}$. The charge and discharge curves of the first, fifth, and tenth cycles show a high degree of similarity, indicating good cycling stability. For the insertion of $Zn^{2+}$, the voltage platforms are formed in the discharge process at 0.32 V. At 0.71 V, the platform is in the charging state, corresponding to the dezincing process. These results indicate good agreement between the GCD test and the CV curve (Fig. 2a and b). At different current densities of 0.1, 0.2, 0.5, 0.8, 1.0, 0.8, 0.5, 0.2, and 0.1 A $g^{-1}$, the corresponding specific discharge capacities are 548.6, 420.2, 345.2, 292.2, 248.9, 304.8, 349.1, 424.3, and 534.1 mA h $g^{-1}$, respectively (Fig. 2c).

The specific capacities of the heterostructures regularly decrease with increasing current density. In contrast, when the current density decreases, the specific capacity increases, proving the excellent rate performance. Fig. 2d shows the cycling performance and the corresponding coulombic efficiency of the heterostructures after 1000 cycles at 0.1 A $g^{-1}$. The initial specific capacity is 679.1 mA h $g^{-1}$, and the specific capacities during the first few cycles are gradually enhanced, which is related to the activation of the heterostructures.[22] After 1000 cycles, the specific capacity is 197.2 mA h $g^{-1}$ and the coulombic efficiency is 91.1%. Furthermore, at a high current density, *i.e.*, 1 A $g^{-1}$, the specific capacity is 192.9 mA h $g^{-1}$ after 300 cycles. These results confirm that the $MoS_2$@C@$Cu_2S$ heterostructures have excellent cycling stability for ZIBs at high current density. In order to investigate the reaction mechanism of $Zn^{2+}$, the electrochemical characteristics of $MoS_2$@C@$Cu_2S$ heterostructures in an aqueous electrolyte were studied using CV in the potential range of 0.2–1.0 V (*vs.* $Zn^{2+}$/Zn). In Fig. 3a, a pair of redox peaks at 0.25/0.75 V is observed, representing the reversible de-intercalation process of $Zn^{2+}$ in $MoS_2$ nanosheets. There is no change in the shape of the CV curves when the scanning rate increases from 0.1 to 1.0 mV $s^{-1}$, which indicates that the heterostructures possess good electrochemical reversibility. With an increased scan rate, the anodic peak moves to a high potential (*i.e.*, 0.76 V) from 0.72 V, and the cathodic peak shifts to a low potential

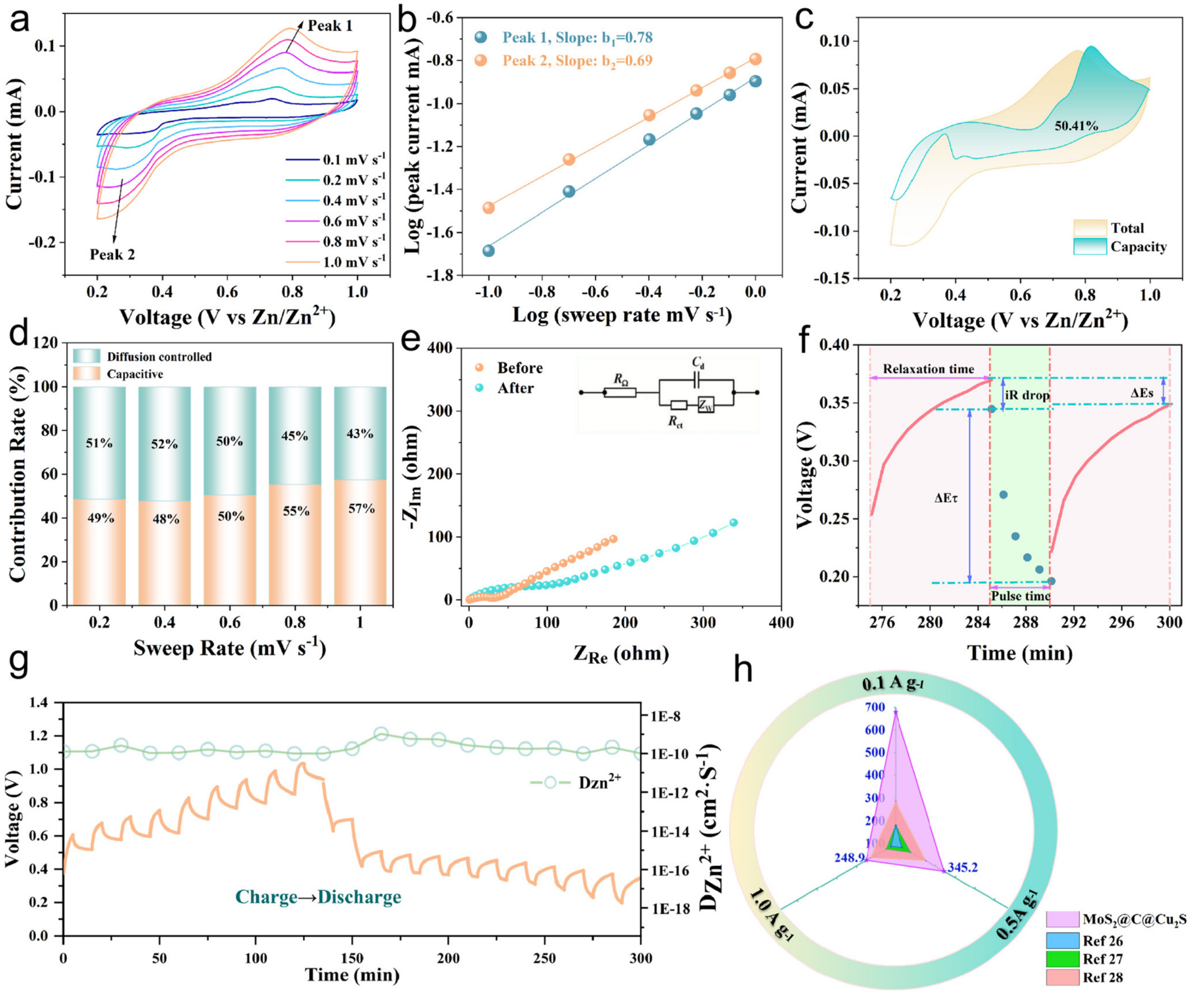

Fig. 3 (a) CV profiles at different scan rates; (b) plot of log (sweep rate) *versus* log (peak current) for anodic and cathodic peaks; (c) the capacitive contribution to the total capacity at 0.6 mV $s^{-1}$; (d) capacity contribution at different scan rates; (e) EIS plots of $MoS_2$@C@$Cu_2S$ heterostructures before and after 100 cycles; (f) GITT test conditions for the heterostructures during the discharge process; (g) GITT profiles and the calculated $D_{Zn}{}^{2+}$ values; (h) comparison of the rate performance with those of previously reported $MoS_2$-based electrode materials applied in ZIBs.

(*i.e.*, 0.25 V) from 0.38 V. These potential changes are related to the enhanced diffusion resistance.

The electrochemical kinetics of the reduction of $Zn^{2+}$ are presented in Fig. 3b. The power formula shows that $I = a\nu^b$, $\log(i) = \log(a) + b\log(\nu)$, where $I$ is the current, $\nu$ is the scanning rate, and $a$ and $b$ are adjustable parameters. The coefficient $b$ represents the type of electrochemical charge storage. When $b$ is in the range of 0.5 to 1, the capacitance controls the process of charge storage.[21] Here, $b$ was calculated to be 0.78 and 0.69 for the oxidation peak and the reduction peak, respectively, indicating that the $Zn^{2+}$ storage process is controlled by a synergistic mechanism between the capacitive contribution and the diffusion process. The contributions of the capacitive effect ($k_1\nu$) and diffusion effect ($k_2\nu^{1/2}$) were further calculated according to the formula: $i = k_1\nu + k_2\nu^{1/2}$. The contribution ratio of the capacitance to the diffusion capacity of the heterostructures was calculated to be ~50.41% at a scan rate of 0.6 mV $s^{-1}$ (Fig. 3c). In Fig. 3d, with the increasing scan rate, *i.e.*, 0.2 to 1.0 mV $s^{-1}$, the capacitance contribution is enhanced from 49% to 57%, indicating that a capacitive-controlled process dominates the storage behavior to promote the rate performance and capacity performance of ZIBs.

Next, electrochemical impedance spectroscopy (EIS) and galvanostatic intermittent titration technique (GITT) tests were executed to evaluate the kinetics of the electrode reaction in detail (Fig. 3e and f). There is a small semicircle diameter in the EIS curves of $MoS_2$@C@$Cu_2S$ heterostructures before and after the cycle (Fig. 3e), indicating that the heterostructures possess good electrical conductivity and rapid $Zn^{2+}$ kinetic diffusion. Based on Fick's second law, the difference in $Zn^{2+}$ diffusion kinetics is explored as follows:

$$D_{Zn^{2+}} = \frac{4}{\tau\pi}\left(\frac{m_B V_M}{S M_B}\right)^2\left(\frac{\Delta E_S}{\Delta E_\tau}\right)^2$$

where $\tau$, $m_B$, $M_B$, $V_M$, and $S$ stand for the current pulse time (s), the mass, the molar mass, the molar volume of active

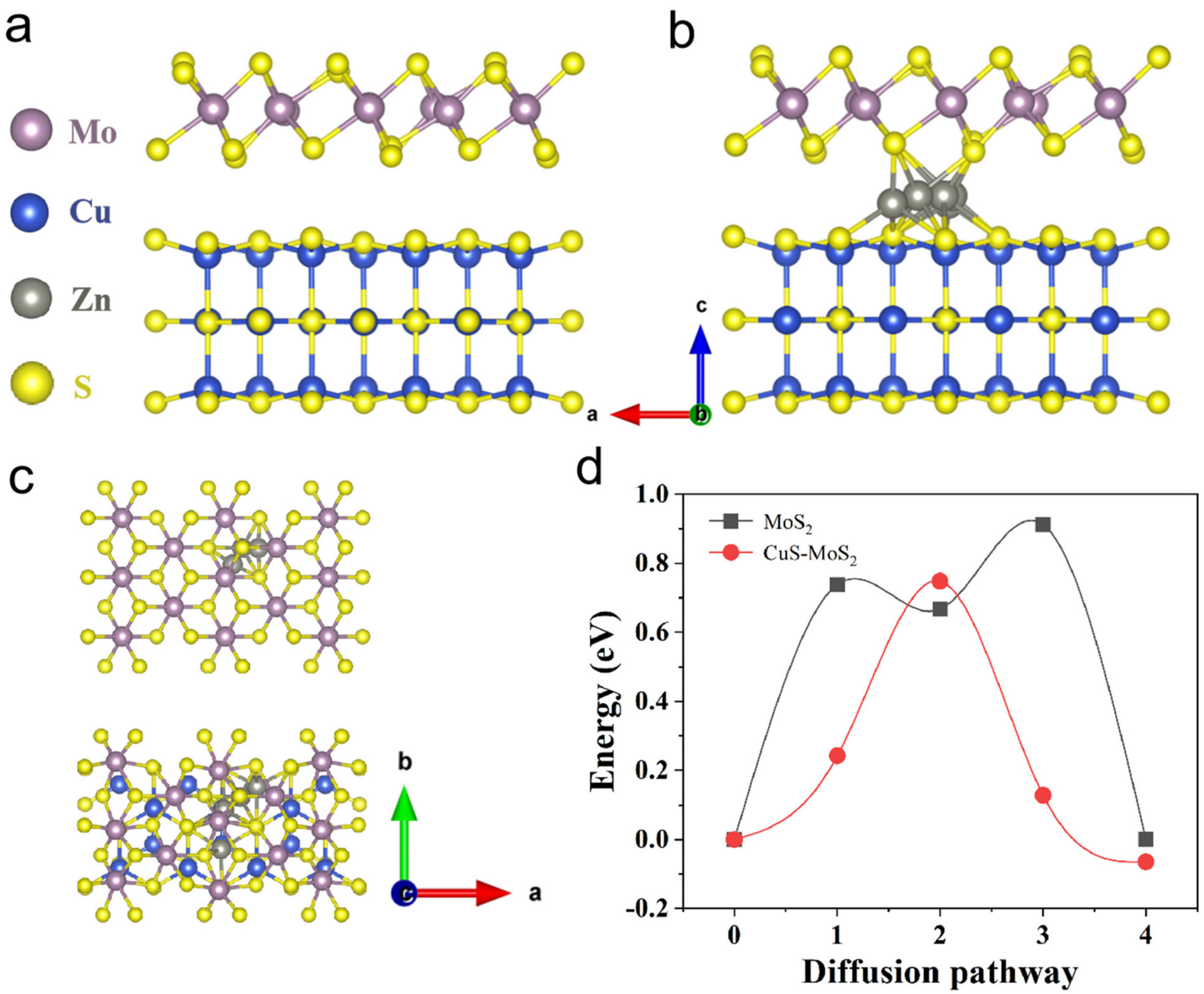

**Fig. 4** (a) Optimized structure of $MoS_2$@C@$Cu_2S$; (b) optimized structure of $Zn^{2+}$ insertion in $MoS_2$@C@$Cu_2S$; (c) top view of the optimized structure of $Zn^{2+}$ insertion in pure $MoS_2$ and $MoS_2$@C@$Cu_2S$; (d) energy barriers of diffusion behavior of $Zn^{2+}$ in pure $MoS_2$ and $MoS_2$@C@$Cu_2S$.

materials, and the area of the electrode, respectively;[23] the calculation method of $\Delta E_S$ and $\Delta E_\tau$ is also displayed in Fig. 3f. It is clearly seen that the pulse time is 5 min, the relaxation time is 10 min, and the quasi-open circuit voltage is reached, and by calculation the $D_{Zn^{2+}}$ was obtained in the range from $10^{-8}$ to $10^{-10}$ cm$^2$ s$^{-1}$ (Fig. 3g), indicating that the electrode possesses good reaction kinetics.[24,25] Compared with previous reports on $MoS_2$-based zinc-ion batteries (Fig. 3h),[26–28] $MoS_2$@C@$Cu_2S$ heterostructures exhibit high performance for ZIBs at different current densities. The excellent electrochemical characteristics of the heterostructures are closely related to the following factors: (1) ultra-thin $MoS_2$ nanosheets cover the surface of hollow C@$Cu_2S$ nanocubes, which would promote fast ion transport and effectively alleviate the volume expansion;[29] (2) the hollow cavity, the high specific surface area (*i.e.*, 34.10 m$^2$ g$^{-1}$), and a large number of electrochemical active sites would shorten the ion diffusion path;[19,25,30] (3) the intermediate C layers maintain the stability of the heterostructures.[26] All three factors enable $MoS_2$@C@$Cu_2S$ heterostructures to achieve superior reversible cycling performance. Density functional theory (DFT) calculations were used to analyze the diffusion of $Zn^{2+}$ inserted in the lattice of $MoS_2$@C@$Cu_2S$ heterostructures at different energy barriers. Fig. 4a exhibits the theoretical laminated structure, and Fig. 4b shows the heterostructure of the interlayer model of $Zn^{2+}$ insertion. Moreover, compared with the $Zn^{2+}$ diffusion barriers of pure $MoS_2$ (Fig. 4c and d), the interlayer diffusion energy barrier of $Zn^{2+}$ decreases in $MoS_2$@C@$Cu_2S$ heterostructures after $MoS_2$ nanosheets grow on the surface of hollow C@$Cu_2S$ nanocubes, which further indicates that the heterostructures are conducive to $Zn^{2+}$ diffusion.

## Conclusions

In summary, novel hollow $MoS_2$@C@$Cu_2S$ heterostructures were fabricated using a template-engaged process for $Zn^{2+}$ storage. These heterostructures with sizes of ~600 nm are packed by folding $MoS_2$ nanosheets and hollow C@$Cu_2S$ nanocubes. Because of the high surface area, *i.e.*, 34.10 m$^2$ g$^{-1}$, these heterostructures exhibit a high initial specific capacity of 679.1 mA h g$^{-1}$ and a reversible capacity of 197.2 mA h g$^{-1}$ with a coulombic efficiency of 91.1% after 1000 cycles at 0.1 A g$^{-1}$. When the capacity was tested at 1.0 A g$^{-1}$, the structure delivered 192.9 mA h g$^{-1}$ after 300 cycles. Furthermore, the hollow heterostructures exhibit excellent rate performance. Therefore, this work provides an effective design of heterogeneous materials for applications in power grid energy storage systems using ZIBs in the future.

## Conflicts of interest

There are no conflicts to declare.

## Acknowledgements

The authors acknowledge the financial support from the Talent Introduction Start-Up Foundation of Guangxi Minzu University (2021KJQD08), the Natural Science Foundation of China (No. 22074130), the Key Scientific Research Projects of Henan Province (232102320040), the National Natural Science Foundation of China (22004032) and the Hunan Provincial Natural Science Foundation of China (2021JJ20020). The authors also acknowledge the great support from the Analysis Testing Center of Xinyang Normal University for materials characterization.

## References

1 X. Xiao, J. Y. Yin, S. Shen, Z. Y. Che, X. Wan, S. L. Wang and J. Chen, Advances in solid-state fiber batteries for wearable bioelectronics, *Curr. Opin. Solid State Mater. Sci.*, 2022, **26**, 101042.

2 H. Yin, K. S. Hui, X. Zhao, S. Mei, X. Lv, K. N. Hui and J. Chen, Eco-Friendly synthesis of self-supported N-Doped $Sb_2S_3$-Carbon fibers with high atom utilization and zero discharge for commercial full Lithium-Ion batteries, *ACS Appl. Energy Mater.*, 2020, **3**, 6897–6906.

3 Q. Zhao, Q. Z. Zhu, J. W. Miao, P. Zhang, P. B. Wan, L. Z. He and B. Xu, Lithium-ion batteries: flexible 3D porous MXene foam for high-performance lithium-ion batteries, *Small*, 2019, **20**, 1970276.

4 X. Xiao, X. Xiao, Y. Zhou, X. Zhao, G. Chen, Z. Liu, Z. Wang, C. Lu, M. Hu, A. Nashalian, S. Shen, K. Xie, W. Yang, Y. Gong, W. Ding, P. Servati, C. Han, S. X. Dou, W. Li and J. Chen, An ultrathin rechargeable solid-state zinc ion fiber battery for electronic textiles, *Sci. Adv.*, 2021, 7, eabl3742.

5 M. Y. Bao, Z. C. Y. Zhang, X. G. An, J. Liu, J. K. Feng, B. J. Xi and S. L. Xiong, Introducing Ce ions and oxygen defects into $V_2O_5$ nanoribbons for efficient aqueous zinc ion storage, *Nano Res.*, 2022, **16**, 2445–2453.

6 G. T. Zan, T. Wu, P. Hu, Y. H. Zhou, S. L. Zhao, S. M. Xu, J. Chen, Y. Cui and Q. S. Wu, An approaching-theoretical-capacity anode material for aqueous battery: Hollow hexagonal prism $Bi_2O_3$ assembled by nanoparticles, *Energy Storage Mater.*, 2020, **28**, 82–90.

7 Z. Z. C. Y. Zhang, B. J. Xi, X. Wang, X. J. Ma, W. H. Chen, J. K. Feng and S. L. Xiong, Oxygen defects engineering of $VO_2 \cdot xH_2O$ nanosheets via in situ polypyrrole polymerization for efficient aqueous zinc ion storage, *Adv. Funct. Mater.*, 2021, **31**, 2103070.

8 H. B. Lu, Z. Z. C. Y. Zhang, X. G. An, J. K. Feng, S. L. Xiong and B. J. Xi, In situ electrochemically transforming VN/$V_2O_3$ heterostructure to highly reversible $V_2NO$ for excellent zinc ion storage, *Small Struct.*, 2023, **4**, 2300191.

9 H. Q. Liu, Y. N. He, H. Zhang, K. Z. Cao, S. D. Wang, Y. Jiang, Q. S. Jing and L. F. Jiao, Lowering the voltage-hys-

teresis of CuS anode for Li-ion batteries via constructing heterostructure, *Chem. Eng. J.*, 2021, **425**, 130548.

10 J. T. Cao, Z. H. Gao, Y. L. Wang, C. Shao, S. W. Ren and Y. M. Liu, Novel Hexagonal Phase Cadmium Sulfide Nanomaterials Based Photoelectrochemical Immunosensor for Sensitive Detection of Prostate Specific Antigen, *J. Xinyang Norm. Univ., Nat. Sci. Ed.*, 2023, **153**, 535–539.

11 J. Xu, Z. Dong, K. J. Huang, L. N. Wang, Z. N. We, L. Yu and X. Wu, Flexible design of large layer spacing V-$MoS_2$@C cathode for high-energy zinc-ion battery storage, *Scr. Mater.*, 2022, **209**, 114368.

12 Y. Li, Z. H. Xing and H. D. Zhang, A novel electrochemical method based on layered tungsten disulfide and Au nanocomposites for the determination of bisphenol, *J. Xinyang Norm. Univ., Nat. Sci. Ed.*, 2022, **35**, 621–625.

13 H. G. Qin, Z. H. Yang, L. L. Chen, X. Chen and L. M. Wang, A high-rate aqueous rechargeable zinc ion battery based on the $VS_4$@rGO nanocomposite, *J. Mater. Chem. A*, 2018, **6**, 23757.

14 L. N. Wang, X. C. Tan, Q. G. Zhu, Z. Dong, X. Wu, K. J. Huang and J. Xu, The universality applications of $MoS_2$@MnS heterojunction hollow microspheres for univalence organic or multivalence aqueous electrolyte energy storage device, *J. Power Sources*, 2022, **518**, 230747.

15 L. X. Fang, M. D. Lan, B. Liu and Y. Cao, Synthesis and electrochemical performance of flower-like, *J. Xinyang Norm. Univ., Nat. Sci. Ed.*, 2022, **35**, 615–620.

16 M. Z. Geng, H. Q. Yang and C. Q. Shang, The multi-functional effects of CuS as modifier to fabricate efficient interlayer for Li-S batteries, *Adv. Sci.*, 2022, **9**, 2204561.

17 X. W. Zhao, Z. C. Liu, W. Y. Xiao, H. Y. Huang, L. H. Zhang, Y. H. Cheng and J. Y. Zhang, Low crystalline $MoS_2$ nanotubes from $MoS_2$ nanomasks for lithium ion battery applications, *ACS Appl. Energy Mater.*, 2020, **3**, 7580–7586.

18 K. Ma, Y. R. Dong, H. Jiang, Y. J. Hu, P. Saha and C. Z. Li, Densified $MoS_2/Ti_3C_2$ films with balanced porosity for ultrahigh volumetric capacity sodium-ion battery, *Chem. Eng. J.*, 2021, **413**, 127479.

19 F. E. Niu, Z. C. Bai, Y. Y. Mao, S. Q. Zhang, H. R. Yan, X. Xu, J. M. Chen and N. N. Wang, Rational design of MWCNTs @ amorphous carbon@$MoS_2$: Towards high performance cathode for aqueous zinc-ion batteries, *Chem. Eng. J.*, 2021, **453**, 139933.

20 S. W. Li, Y. C. Liu, X. D. Zhao, Q. Y. Shen, W. Zhao, Q. W. Tan, N. Zhang, P. Li, L. F. Jiao and X. H. Qu, Sandwich-like heterostructures of $MoS_2$/Graphene with enlarged interlayer spacing and enhanced hydrophilicity as high-performance cathodes for aqueous Zinc-ion batteries, *Adv. Mater.*, 2021, **33**, 2007480.

21 F. Shao, Y. F. Huang, X. L. Wang, Z. J. Li, X. D. Huang, W. T. Huang, L. B. Dong, F. Y. Kang, W. B. Liu and C. Xu, $MoS_2$ with high 1T phase content enables fast reversible zinc-ion storage via pseudocapacitance, *Chem. Eng. J.*, 2022, **448**, 137688.

22 S. M. Xu, X. Liang, X. Y. Wu, S. L. Zhao, J. Chen, K. X. Wang and J. S. Chen, Multistaged discharge constructing heterostructure with enhanced solid-solution behavior for long-life lithium-oxygen batteries, *Nat. Commun.*, 2019, **10**, 5810.

23 Z. H. Jin, X. B. Hu, L. J. Xu, Y. P. Xie and Z. W. Zhang, Synthesis and characterization of Co-Ni-S/MXene composite electrode materials for supercapacitor performance, *J. Xinyang Norm. Univ., Nat. Sci. Ed.*, 2023, **153**, 540–543.

24 Y. Q. Teng, H. L. Zhao, Z. J. Zhang, Z. L. Li, Q. Xia, Y. Zhang, L. N. Zhao, X. F. Du, Z. H. Du, P. P. Lv and K. Świerczek, $MoS_2$ nanosheets vertically grown on graphene sheets for Lithium-ion battery anodes, *ACS Nano*, 2016, **10**, 8526–8535.

25 X. Wang, Z. Z. C. Y. Zhang, M. Huang, J. K. Feng, S. L. Xiong and B. J. Xi, In situ electrochemically activated vanadium oxide cathode for advanced aqueous Zn-Ion batteries, *Nano Lett.*, 2022, **22**, 119–127.

26 H. Wang, X. Lan, D. Jiang, Y. Zhang, H. Zhong, Z. Zhang and Y. Jiang, Sodium storage and transport properties in pyrolysis synthesized $MoSe_2$ nanoplates for high performance sodium-ion batteries, *J. Power Sources*, 2015, **283**, 187–194.

27 L. Zeng, Y. Fang, L. Xu, C. Zheng, M.-Q. Yang, J. He, H. Xue, Q. Qian, M. Wei and Q. Chen, Rational design of few-layer $MoSe_2$ confined within ZnSe-C hollow porous spheres for high-performance lithium-ion and sodium-ion batteries, *Nanoscale*, 2019, **11**, 6766–6775.

28 T. S. Wang, D. Legut, Y. C. Fan, J. Qin, X. F. Li and Q. F. Zhang, Building fast diffusion channel by constructing metal sulfide/metal selenide heterostructures for high-performance sodium ion batteries anode, *Nano Lett.*, 2020, **20**, 6199–6205.

29 X. Zhang, X. Li, J. Liang, Y. Zhu and Y. Qian, Synthesis of $MoS_2$@C nanotubes via the kirkendall effect with enhanced electrochemical performance for lithium ion and sodium ion batteries, *Small*, 2016, **12**, 2484–2491.

30 H. Q. Liu, J. J. Fu, X. X. Wang, Y. Guo, X. Gong, Z. H. Jin and K. Z. Cao, Preparation and SERS property of PVDF self-powered flexible substrate, *J. Xinyang Norm. Univ., Nat. Sci. Ed.*, 2023, **152**, 385–389.